# Vortex phase diagram of the kagome superconductor $CsV_3Sb_5$

Xinyang Zhang,[1,2,3] Mark P. Zic,[2,4] Dong Chen,[5,6] Chandra Shekhar,[5] Claudia Felser,[5] Ian R. Fisher,[1,2,3] and Aharon Kapitulnik[1,2,3,4]

[1]*Stanford Institute for Materials and Energy Sciences, SLAC National Accelerator Laboratory, 2575 Sand Hill Road, Menlo Park, California 94025, USA*

[2]*Geballe Laboratory for Advanced Materials, Stanford University, Stanford, California 94305, USA*

[3]*Department of Applied Physics, Stanford University, Stanford, California 94305, USA*

[4]*Department of Physics, Stanford University, Stanford, California 94305, USA*

[5]*Max Planck Institute for Chemical Physics of Solids, 01187 Dresden, Germany*

[6]*College of Physics, Qingdao University, Qingdao 266071, China*

(Received 1 November 2023; revised 18 February 2024; accepted 20 March 2024; published 8 April 2024)

The screening response of the kagome superconductor $CsV_3Sb_5$ was obtained from high-resolution ac mutual inductance measurements. At zero applied magnetic field and low temperatures, we observe no evidence for gapless quasiparticles, while near $T_c$ we find evidence for enhanced fluctuations. A rich vortex state appears above $H_{c1} \approx 30$ Oe, exhibiting successive emergence of vortex phases. For a fixed magnetic field, lowering the temperature below $T_c(H)$ leads to a wide range of vortex liquid state in a landscape of weak pinning potential, which gives rise to an irreversibility line. Further lowering the temperature, we identify the vortex melting line followed by the peak effect manifested in enhanced vortex pinning strength and critical current. We suggest that such an unusual behavior, where the peak effect region is fully contained within the vortex lattice state below the irreversibility line, is a consequence of the strong anisotropy and weak bulk pinning in $CsV_3Sb_5$.

DOI: 10.1103/PhysRevB.109.144507

## I. INTRODUCTION

Correlated metals in reduced dimensions often exhibit propensity to multiple ordered phases with similar energies, which leads to the phenomenon of intertwined order [1–3], where multiple phases emerge out of a primary phase. Kagome metals, featuring correlated electron effects and a topologically nontrivial band structure, have recently emerged as a compelling family of compounds to realize such multiple ordered electronic states. A particularly interesting material system in that respect is the class of quasi-two-dimensional kagome metals $AV_3Sb_5$, which exhibit charge-order transitions at ∼80 K, 103 K, and 94 K for $A$ = K, Rb, and Cs, respectively [4]. Focusing on $CsV_3Sb_5$, a charge density wave (CDW) transition is revealed which is associated with a substantial reconstruction of the Fermi surface pockets linked to the vanadium orbitals and the kagome lattice framework [5]. Nuclear magnetic resonance studies on the different vanadium sites is consistent with orbital ordering at $T \sim 94$ K induced by a first-order structural transition, accompanied by electronic CDW that appears to grow gradually below $T_{CDW}$, with possible intermediate subtle stacking transitions perpendicular to the kagome planes [6].

The appearance of superconductivity with $T_c$ ranging from ∼2.5 K to 4 K prompted further examinations of the relation between the normal and the superconducting states [7,8], with initial studies suggesting a pair-density-wave [9]. While the possibility of a time-reversal symmetry breaking CDW state [10] is still under debate [11], the emerging superconducting state appears to exhibit a gapped conventional $s$-wave order parameter [10]. With in-plane $H_{c2}$ clearly dominated by orbital effects and a large Ginzburg-Landau parameter (in our experiment, we estimated $\kappa \sim 28$), we might expect a rather ordinary vortex physics behavior. Considering the nontrivial topological band structure of $CsV_3Sb_5$, Majorana zero mode (MZM) excitations in vortex cores [12] may be expected. However, it is not yet clear whether there exists a range of magnetic fields where vortex-induced MZMs do not fade out due to overlap and thus affect the observed $H$-$T$ phase diagram of this material.

In this paper, we examine the vortex phase diagram of $CsV_3Sb_5$ through measurements of the superfluid response using a high-resolution mutual-inductance (MI) probe, supplemented by resistivity and magnetization measurements (Appendices D and E). Whereas the low-temperature zero-field data confirms the absence of gapless quasiparticles, we find an unusually wide temperature range of phase fluctuations, which at a finite magnetic field evolves into a wide vortex liquid phase. For a constant magnetic field, an irreversibility line is observed, separating unpinned dissipative vortex liquid from a weak pinning regime characterized by weak sensitivity to the measurement timescale. The vortex lattice melting transition, appearing at lower fields and temperatures, is identified as an abrupt increase in inductive response. Finally, a pronounced peak effect is observed below the melting transition, exhibiting a hysteresis that weakens with increasing temperature. We therefore observe that $CsV_3Sb_5$ provides a unique example of a clean anisotropic superconductor where a hierarchical succession of transitions and crossovers in the vortex state do not cross each other (by contrast to, e.g., $Bi_2Sr_2CaCu_2O_{8+y}$ [13]) and where the melting point is clearly distinct from other effects (by contrast

 

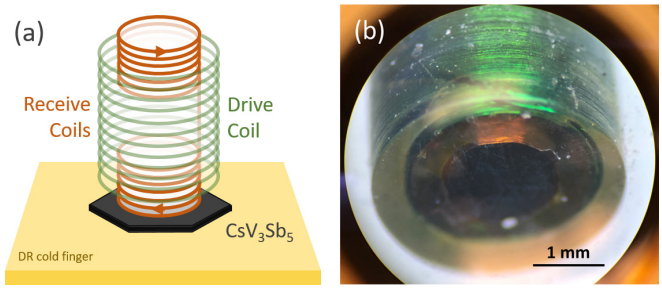


FIG. 1. The mutual inductance (MI) measurement. (a) Simplified 3D view of the MI probe mounted over a $CsV_3Sb_5$ sample, which is thermally anchored by a thick puddle of silver paint onto the mixing chamber of a dilution refrigerator. (b) Bottom view of the MI probe under the microscope. The green-colored drive coil and bronze-colored receive coils were cast in epoxy, which is polished to ∼20 μm between the wires and the bottom surface. The scale bar indicates 1 mm.

to, e.g., $YBa_2Cu_3O_{7-y}$ [14]). Taking into account the strong anisotropy $\gamma \sim 10$ of $CsV_3Sb_5$ [4,15], we calculate a low-temperature limit for vortex-entropy change as ∼0.02 $k_B$ per layer.

The peak effect is often observed in the inductive part of superfluid response, while exhibiting an enhancement in the depinning critical current density $j_c$ near $H_{c2}$ [16]. Typically accompanied by a hysteresis, it is closely linked to the strengthening of pinning in a vortex glass regime [17,18]. Such effects have been under scrutiny in a broad range of type-II superconductors, including Nb(O, Ti) [19], NbZr [20], $YBa_2Cu_3O_{7-\delta}$ [21,22], 2H-$NbSe_2$ [23], (Ba, K)$Fe_2As_2$ [24], and ternary stannide $Ca_3Rh_4Sn_{13}$ [25], as well as germanides $Lu_3Os_4Ge_{13}$ and $Y_3Ru_4Ge_{13}$ [26]. Different scenarios for the interplay between vortex pinning and lattice elasticity defines melting and irreversibility lines, which play important roles in determining the magnetic properties of high-$T_c$ cuprates such as $YBa_2Cu_3O_7$ and $Bi_2Sr_2CaCu_2O_8$ [27], often led to conflicting phase diagrams, particularly in discerning the thermodynamic melting transition out of the pinning-induced vortex state. The clear feature that we observe between the irreversibility line and the peak effect is unique in that respect, especially as it seems to mark the melting transition.

## II. METHODS AND MATERIAL

We adopt the MI technique as an alternative approach of measuring the complex ac superfluid response [28,29]. In zero external magnetic field, the screening response due to a small ac drive can be related to superfluid density and (effective) penetration depth, given exact geometries of the sample and MI coils [30]. In the present paper, the complex ac response $V = V' - iV''$ of superconducting $CsV_3Sb_5$ single crystals was measured using a gradiometer-type MI probe [29], as shown in Fig. 1. In this configuration, both the drive coil and the astatically wound pair of receive coils (1.5 mm in diameter) are positioned above the sample. The drive coil is supplied an ac current of 20 μA at 100 kHz, thus creating a minuscule ac magnetic field $H_{ac} \lesssim 3$ mOe $\ll H_{c1}$ and inducing screening supercurrents (and potentially dissipations) in the superconductor; meanwhile, the receive coils pick up

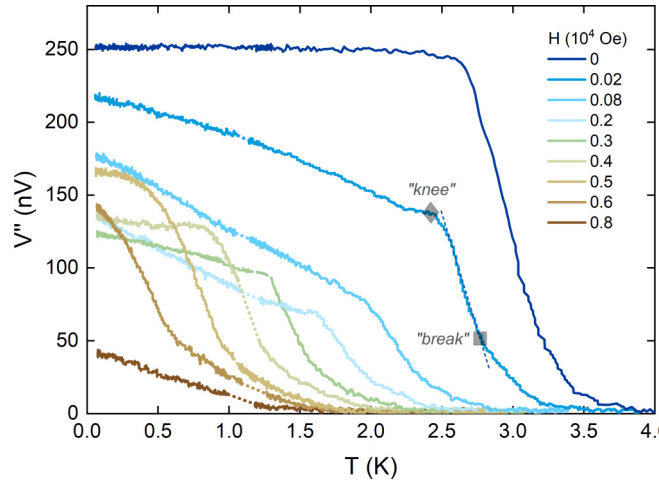


FIG. 2. Temperature dependence of inductive response $V''(T)$ in varying perpendicular magnetic field. Dotted lines connect data <1 K and >1.2 K. A "knee" feature is apparent in almost every curve and its location is nonmonotonic as field increases. Above the knee, a rapid linear drop in signal crosses over to a more gradual decrease to zero, separated by a break in behavior. For further explanations, see Fig. 4.

both quadratures $V'$ and $V''$ of the induced emf using a lock-in amplifier phase-locked at the drive frequency.

$CsV_3Sb_5$ single crystals were prepared by the self-flux method [4,31]. An approximately $2 \times 2 \times 0.1$ mm$^3$ hexagonal-shaped $CsV_3Sb_5$ crystal was silver pasted onto the cold finger of a dilution refrigerator, where the MI coils are mounted above and gently pressed down onto the sample. Care was taken to minimize the stress exerted by the coil assembly, which together with the measurement wiring is well thermalized at the mixing chamber temperature. Details of the coil assembly can be found in the Supplemental Material [32].

## III. RESULTS

### A. The superconducting transition

We first focus on the superconducting transition in zero magnetic field as shown in Fig. 2. With careful tuning of the applied magnetic field such that any effect of remnant field is eliminated, we identify a zero-field superconducting transition temperature $T_c(H = 0) \approx 4.0$ K, where the onset of inductive response $V''$ at 100 kHz is located. Following a gradual increase of $V''(T)$ over a transition region of $\Delta T/T_c \sim 1/4$, the inductive signal saturates at the maximum value below $T \lesssim 2$ K. The finite size of the sample with respect to our coils limited our ability to extract a penetration depth $\lambda(T) \propto T^{-0.5} \exp(-\Delta(0)/T)$ or a superfluid density $n_s(T) \propto \lambda^{-2}(T)$ from the measured $V''(T)$. Nevertheless, such temperature independence as $T \to 0$ is supported by the recent measurements of penetration depth that yielded similar results, i.e., nodeless superconductivity exhibiting no signature of gapless quasiparticles in zero magnetic field [33,34].

Upon applying a dc magnetic field along the $c$ axis $H_{dc} > H_{c1\|c} \approx 30$ Oe at 0.12 K, the inductive response $V''(T)$ is increasingly suppressed and becomes temperature dependent as $T \to 0$ in Fig. 2. From the measured $H_{c1\|c}$ and an

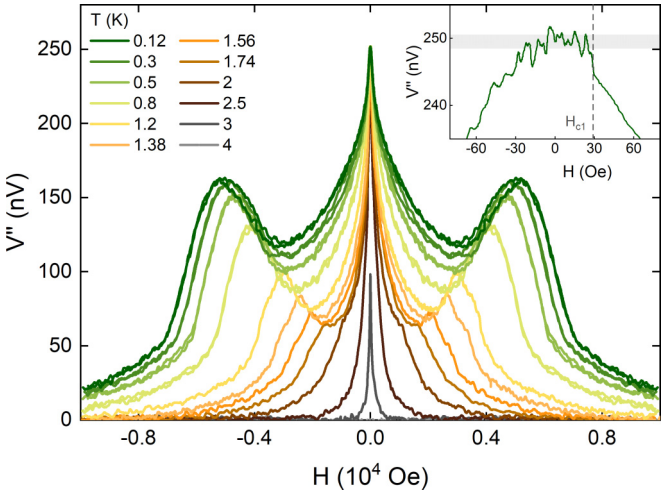


FIG. 3. Magnetic field dependence of inductive response isotherms $V''(H)$ at different temperatures. External magnetic field is along the $c$ axis perpendicular to the V plane. For temperature below 0.5 K, both up sweeps and down sweeps are plotted. The most prominent hysteresis is at the low-field edges of the peaks, which altogether forms an envelope shape. Note the highly symmetric shape in positive and negative fields. Inset: Expanded view of $V''(H)$ in low fields showing field-independent screening response as a signature of the Meissner state. The shadow indicates experimental uncertainty ~2 nV.

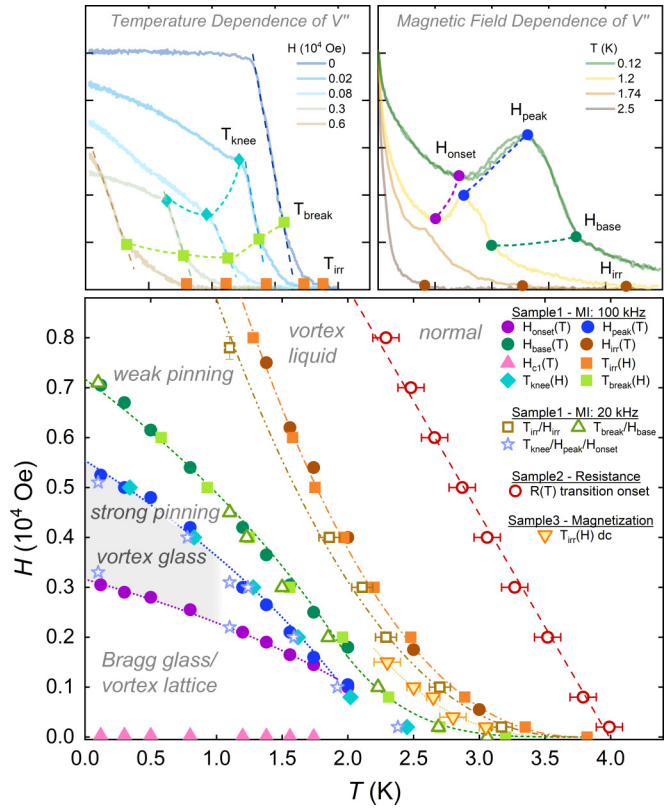


FIG. 4. Vortex phase diagram of $CsV_3Sb_5$. Top left: Temperature dependence of $V''$ at select fields showing the extraction of $T_{knee}$, $T_{break}$, and $T_{irr}$. Top right: Magnetic-field dependence of $V''$ at select temperatures showing the extraction of $H_{onset}$, $H_{peak}$, $H_{base}$, and $H_{irr}$. Bottom: $H$-$T$ phase diagram constructed by the extracted features, including those from 20-kHz MI measurements (Appendix C). The yellow triangles were extracted from dc magnetization. The shadow marks the region with strong hysteresis. The mean-field $T_{c0}/H_{c2}$ (red circle) is extracted from the onset of a superconducting transition in resistance measurements when resistance begins to drop below the normal state value (Appendix D). Fitting of the mean-field transition $T_{c0}/H_{c2}$ to the WHH formula [36] yields $\xi(0) \approx 16$ nm. Feature extractions have uncertainties of order ~0.01 K in temperature or ~100 Oe (100 kHz)/500 Oe (20 kHz) in field (error bars suppressed for clarity except for $H_{irr}$ and $T_{c0}$). Dashed lines are guides to the eye.

estimated $H_{c2\|c}$ [15], we find the in-plane penetration depth $\lambda_{ab} = \sqrt{\Phi_0[\ln(\lambda/\xi) + 0.5]/4\pi H_{c1\|c}} \approx 450$ nm (see Fig. 4 for our estimate of $H_{c2\|c}$ and Appendix A), consistent with the tunneling diode oscillator method [33]. In intermediate fields 2 kOe $\lesssim H \lesssim$ 6 kOe, the evolution of $V''(T)$ appears nonmonotonic as a function of magnetic field. For each curve below 6 kOe, there also appears to be a "knee" marking a change in slope and a "break" that separates a gradual superconducting transition at high temperatures and a more rapid linear form at intermediate temperatures. Above 6 kOe, $V''(T)$ drops monotonically to zero as the inductive superfluid response is increasingly suppressed. We will examine such a nonmonotonic evolution in details by exploring the magnetic-field-dependence of $V''$ isotherms.

### B. Magnetic-field dependence of the superfluid response

In Fig. 3, isothermal field sweeps in $CsV_3Sb_5$ demonstrate a broad array of qualitative features related to various vortex states. Below a lower critical field $H_{c1} \sim 30$ Oe at low temperatures, the inductive ac response $V''(H)$ is independent of magnetic field as in the Meissner state. Above $H_{c1}$, $V''(H)$ drops sharply, corresponding to a rapidly weakening screening response, until a peak develops in each of the inductive response isotherms below ~2 K. These peaks span a wide portion of the intermediate field range and correspond to the nonmonotonic behavior in the temperature-dependence, reminiscent of the widely known peak effect [16,19,20,23–27].

The peaks in $CsV_3Sb_5$ appear more prominent at lower temperatures, approaching 30% of the maximal zero-field signal, while a peak was also found in critical current measurements [32]. The peak's onset field ($H_{onset}$), peak field ($H_{peak}$), and width ($|H_{base} - H_{onset}|$) all increase with lower temperature, consistent with the canonical peak effect behaviors. Nevertheless, the peaks in $CsV_3Sb_5$ are located at an intermediate range of magnetic field rather than close to the onset of screening response at higher fields.

Hysteresis in $V''(H)$ is largely seen at the low-field edges of the peaks with the largest split of ~7 nV between upward and downward sweeps, and can be detected until at least 0.8 K, where the split drops below measurement sensitivity. There also exists a much weaker hysteresis at lower fields (see Appendix B). Such a hysteresis has been identified as a signature of the vortex glass phase [18,35]. In addition, the low-field edges of the peaks in all isotherms together form an envelope, corresponding to a weak temperature dependence near the knees in Fig. 2.

## IV. DISCUSSIONS

The rich features in the temperature- and field dependence of superfluid screening response $V''$ allow us to identify various vortex phases in an $H$-$T$ phase diagram Fig. 4. Close to zero magnetic field, the Meissner state with a constant diamagnetic susceptibility is bounded by the low $H_{c1} \sim 30$ Oe and is barely visible. From the field-dependence $V''(H)$, we extract the peak's onset $H_{\text{onset}}(T)$ (violet), peak $H_{\text{peak}}(T)$ (blue), and base $H_{\text{base}}(T)$ (green) as a function of temperature. Independently, from the temperature-dependence $V''(T)$, we extract $T_{\text{knee}}(H)$ (light blue) and $T_{\text{break}}(H)$ (light green) as a function of field as explained previously. The resulting curves are surprisingly consistent with each other, where $T_{\text{knee}}(H)$ and $H_{\text{peak}}(T)$ as well as $T_{\text{break}}(H)$ and $H_{\text{base}}(T)$ are perfectly aligned, respectively. The peaks become indistinguishable above $\sim 0.5T_c \approx 2$ K.

### A. Peak effect and vortex glass phase

We begin with the low-field and low-temperature regimes of the $H$-$T$ phase diagram. The strong hysteretic behavior (shadow) is bounded between $H_{\text{onset}}(T)$ (violet) and $H_{\text{peak}}(T)$ (blue), with its magnitude dropping below our sensitivity above $\sim 1$ K. Consequently, $H_{\text{onset}}$ can be designated as the onset of a strongly hysteretic vortex glass phase, replacing a less-disordered dislocation-free Bragg glass phase at lower fields [18]. The vortex glass region is highly correlated with the peaks in the screening response $V''(H)$, which signifies an enhancement in flux pinning [25]. Such an enhancement is commonly achieved through a crossover from the Larkin-Ovchinnikov collective pinning to individual pinning of the flux lines, following the softening of vortex lattice elastic moduli [17] in the presence of a significant anisotropy [15].

In previous studies of the vortex phase diagram in layered materials, particularly the cuprates, a gradual evolution in pinning strength is commonly expected between the boundary of the peak effect at $H_{\text{peak}}$ and $H_{\text{irr}}$. In these cases and with no otherwise observable features, $H_{\text{peak}}$ is identified with the melting transition (see, e.g., Refs. [23,37].) However, where a magnetization discontinuity is observed without a peak effect, a melting line was found to cross the irreversibility line in $Bi_2Sr_2CaCu_2O_8$ [13]. In the present case of $CsV_3Sb_5$, we find a pronounced break in the response of the vortex system between $H_{\text{peak}}$ and $H_{\text{irr}}$, which we denote as $H_{\text{base}}(T)$. This feature is also visible in the temperature scans of the inductive response, which we identify as $T_{\text{break}}(H)$. Such a break was previously found in surface impedance measurements of $Bi_2Sr_2CaCu_2O_8$ [38] and was identified with the melting line. Similar to our case, their technique, while performed at higher frequency, was sensitive to the superfluid density, which is expected to exhibit a sharp increase in superfluid density as the field is lowered through the melting transition. It is therefore natural to identify the line of $[T_{\text{break}}(H), H_{\text{base}}(T)]$ as the melting transition [39]. This now allows us to calculate the entropy change through the transition. Following Zeldov *et al.*, [40], we can use the Clausius-Clapeyron equation to calculate the latent heat of the transition: $L = T_m \Delta S = -(\Delta B/4\pi)(dH_m/dT)T_m$, where $(T_m, H_m)$ is the melting line and $\Delta B$ is the discontinuity in magnetic induction at the first-order melting transition. Using a standard Lindeman criterion for melting [39] to estimate $\Delta B$, we find [40] $\Delta S \approx 0.1 d\gamma\sqrt{B_m/\Phi_0}$, where $\gamma \approx 10$ is the anisotropy of $CsV_3Sb_5$ [15] and $d \approx 9.3$ Å is the interlayer distance [4]. At low temperatures and high fields, we find that $\Delta S \sim 0.02\ k_B$ per kagome layer, which is a factor of $\sim$10 smaller than the expected value from fully decoupled layers [41]. This implies correlations along the vortex line, which thus limit the number of degrees of freedom per vortex.

Returning to the peak effect, when compared with typical characteristics in both layered and nonlayered superconductors [19–26], the peak effect in $CsV_3Sb_5$ appears more prominent and spans a large range in parameter space. The details of pinning mechanisms are still unclear in $CsV_3Sb_5$, whether being randomly distributed pointlike impurities or correlated effects related to the underlying CDW and its associated distortions. However, at least down to $\sim T_c/2$, the temperature dependence of the irreversibility line and peak effect line follow the melting line, which could indicate that in that regime, surface barrier effects are not important and bulk pinning dominate [13].

### B. Irreversibility line

In the high-field and high-temperature regimes, we attribute the onset of $V''$ $[H_{\text{irr}}(T)]$, for different frequencies, including dc, to the presence of pinned vortices, and thus an ac irreversibility line or depinning line $H_{\text{irr}}(T) \sim (T_c - T)^{\alpha}$, where the exponent typically ranges from $\frac{4}{3}$ to 2 [27]. As we are measuring the response of a coherent sum of screening currents over a select range of wave vectors determined by the receive coil geometry [29] and over a timescale determined by the drive frequency, our measurement is mostly sensitive to flux lines that appear pinned within the experiment's parameters. In that respect, the region bounded by the irreversibility and peak effect lines indicate the increase in pinning efficiency, starting from thermally activated flux flow [42] at high temperatures, with its hallmark of frequency dependence (see Fig. 4), to the strong pinning in the peak effect regime with intermediate change in pinning behavior below the freezing of the vortex lattice.

Finally, we note that debates persist for an unambiguous identification of the irreversibility line since it is highly sensitive to either geometrical barriers or the external drive current that causes depinning of vortices [13,27]. It is important to note that the drive field in our experiment is several orders of magnitude lower compared to typical ac susceptibility measurements at $\sim$1 Oe, whereas our MI experiment is complementary to transport measurements that typically require much higher drive current. Further clarifications on the irreversibility line may be achieved through torque magnetometry [43] or local magnetic induction experiments [13].

## V. SUMMARY

In summary, the screening response of vortices in kagome superconductor $CsV_3Sb_5$ has been measured using the ac MI technique. Besides confirming the absence of gapless

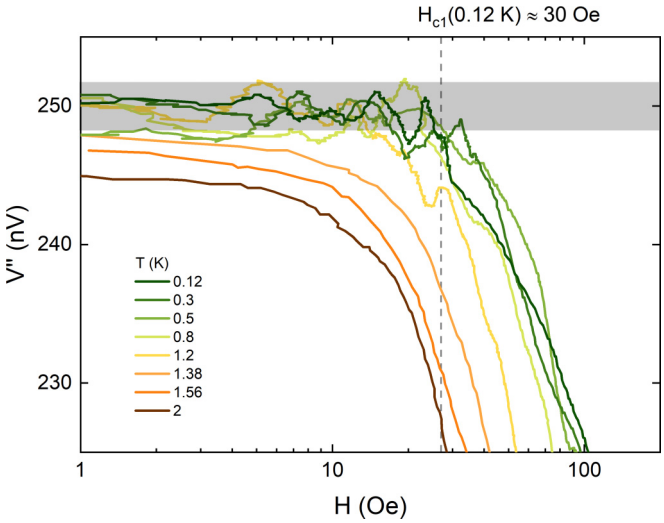


FIG. 5. Inductive response $V''(H)$ as a function of magnetic field measured at 100 kHz. The shadow marks experimental uncertainty ∼2 nV. The lower critical field at 0.12 K is identified at ≈30 Oe.

quasiparticles in zero external magnetic field, we observe the peak effect, corresponding to enhanced pinning strength and critical current, in a broad intermediate range of magnetic field. The peaks vanish at a melting transition from strong to weak pinning, unlike the usual peak effect that ends near $H_{\rm irr}$ or $H_{c2}$. Hysteresis in $V''$ leads us to the identify a vortex glass phase, where its onset is highly correlated with that of the peaks. The various features in the temperature and field dependence of the screening response, corroborated by transport and dc magnetization measurements, have allowed us to construct an $H$-$T$ phase diagram of the vortex states and to infer the irreversibility line $H_{\rm irr}(T)$.

## ACKNOWLEDGMENTS

Work at Stanford University was supported by the Department of Energy, Office of Basic Energy Sciences, under Contract No. DE-AC02-76SF00515. M.P.Z. was partially supported by the National Science Foundation under Grant No. DGE-1656518. The authors gratefully acknowledge (financial) support by the Deutsche Forschungsgemeinschaft through SFB 1143 (Project-ID No. 258499086) and through the Würzburg-Dresden Cluster of Excellence on Complexity and Topology in Quantum Matter ct.qmat (EXC 2147, Project-ID No. 39085490).

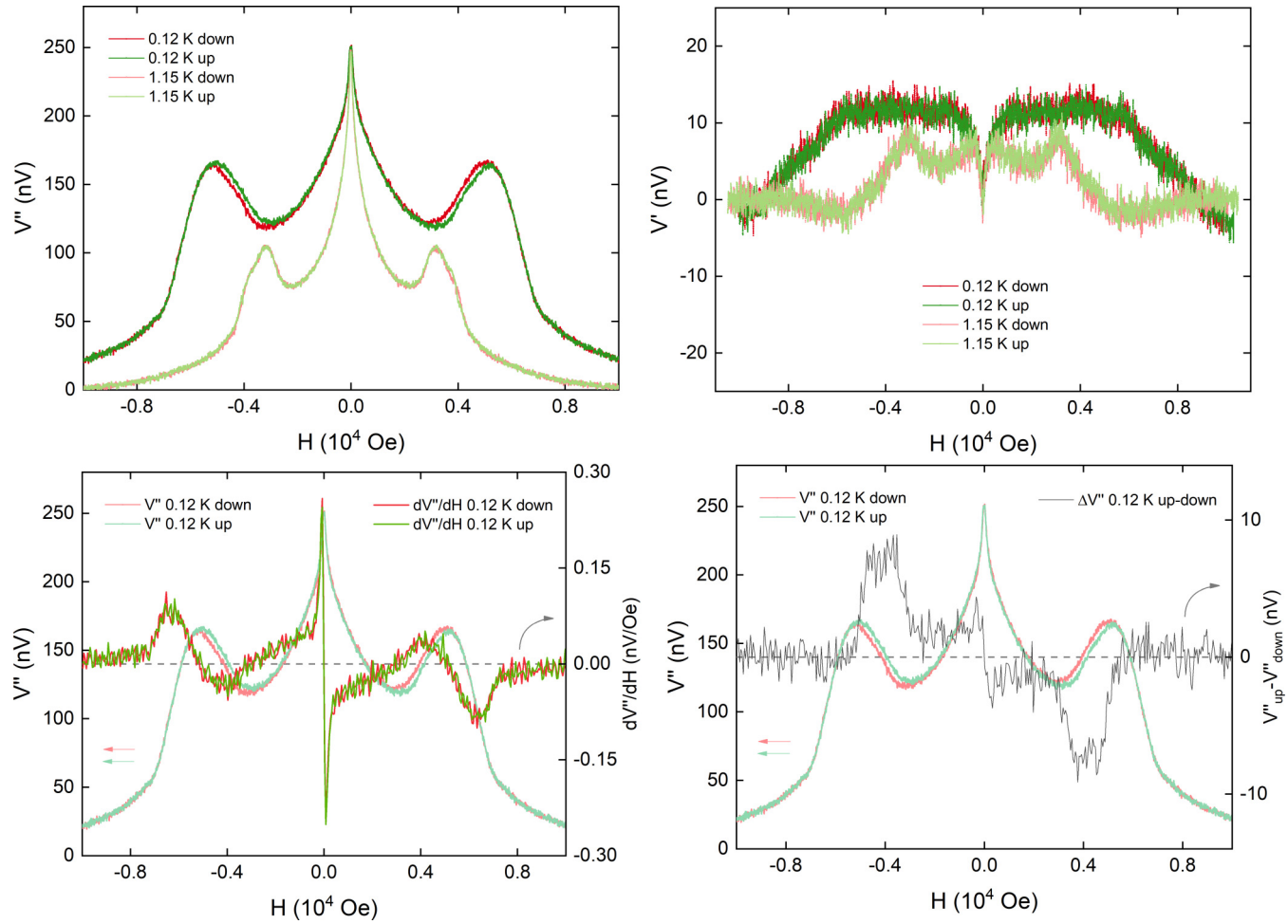


FIG. 6. Inductive (screening; upper left) and dissipative (upper right) response of $CsV_3Sb_5$ as a function of external magnetic field at different temperatures. Data taken with the same drive current as in the main text Fig. 3 at 100 kHz. Lower left: First-order derivative $dV''/dH$ at 0.12 K, overlaid with $V''(H)$. Lower right: Hysteresis split $\Delta V''_{\rm u\text{-}d}$ at 0.12 K, overlaid with $V''(H)$.

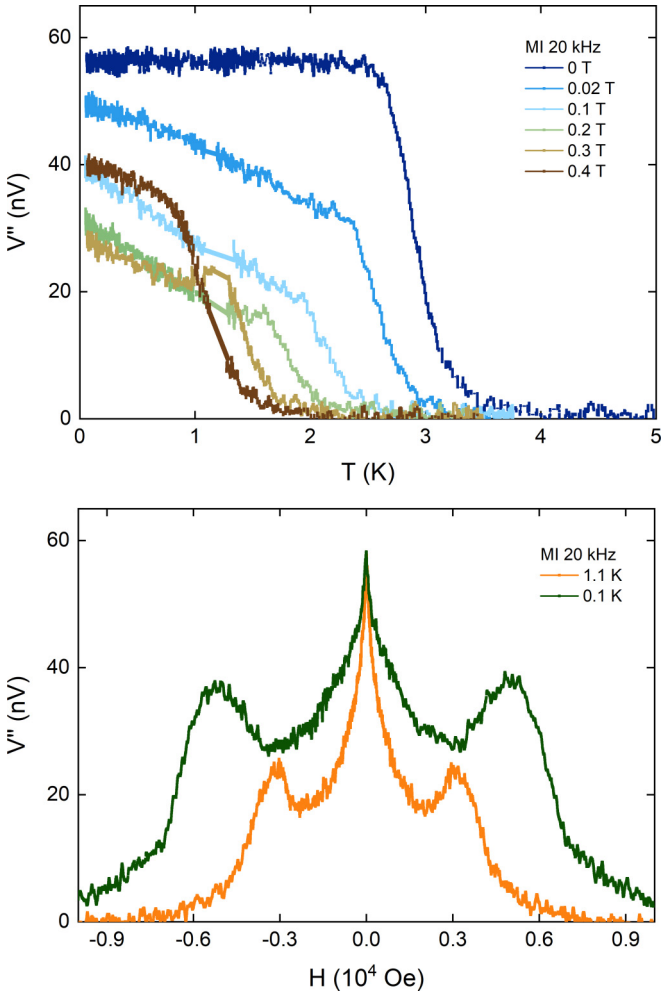


FIG. 7. Temperature and field dependencies of inductive (screening) response of $CsV_3Sb_5$ at 20 kHz.

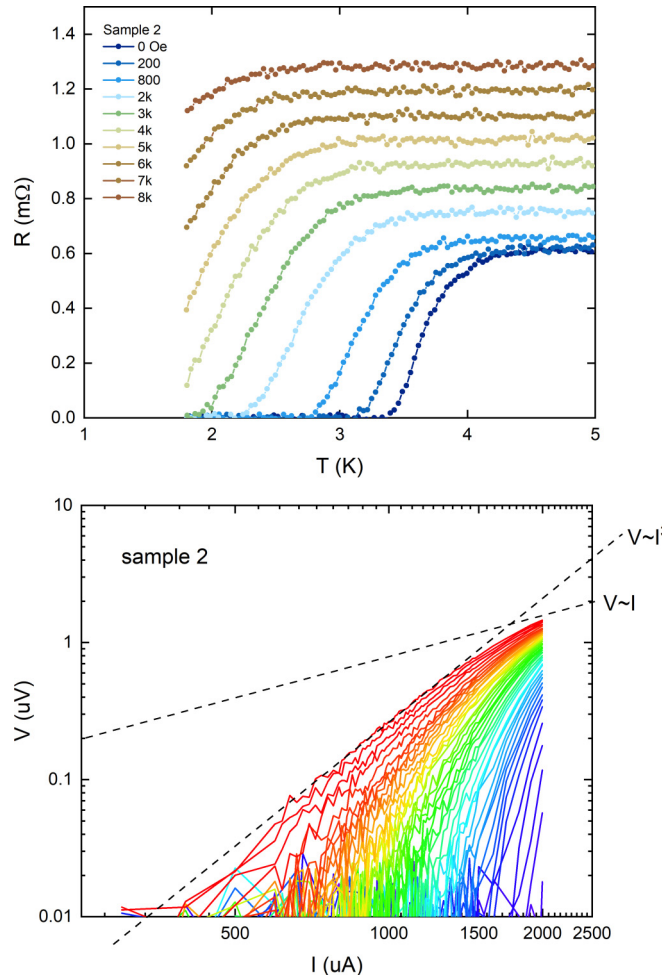


FIG. 8. Resistance vs temperature in different magnetic fields and I-V characteristics at 1.88 K of $CsV_3Sb_5$ (sample 2). Applied magnetic field ranges from 0 Oe (violet) to 3 kOe (red).

## APPENDIX A: DETAILED LOW-FIELD INDUCTIVE RESPONSE $V''(H)$ AND THE EXTRACTION OF EFFECTIVE PENETRATION DEPTH

As shown in Fig. 5, the lower critical field is defined in the presence of anisotropy as $H_{c1} = (\Phi_0/4\pi\lambda^2)[\ln(\lambda/\xi) + 0.5]$, where $\Phi_0 = h/2e$ is the magnetic flux quantum, $\lambda$ is the penetration depth, and $\xi$ is the coherence length. By taking the experimentally determined in-plane coherence length $\xi_{ab}(T = 0) \approx 16$ nm, we consider the $c$-axis lower critical field

$$H_{c1\|c} = \frac{\Phi_0}{4\pi\lambda_{ab}^2}\left(\ln\frac{\lambda_{ab}}{\xi_{ab}} + 0.5\right) \approx 30\ \text{Oe}, \qquad \text{(A1)}$$

which yields an (measured) in-plane penetration depth $\lambda_{ab} \approx 450$ nm.

## APPENDIX B: HIGH-QUALITY MEASUREMENTS OF HYSTERESIS IN FIELD-DEPENDENT SCREENING RESPONSE

To improve data quality and to reduce the effect of the finite time constant in lock-in detection, we repeated the field-dependent measurement at a much lower field ramp rate of ∼1 Oe/s in both ramp directions. For reference, the feature size relevant to the peak effect is ∼1000 Oe. This allows us to calculate the first-order derivative versus magnetic field $dV''/dH$. The local maxima/minima can be pinpointed, whereas a peak in $dV''/dH$ at $\sim \pm 6.5$ kOe corresponds to the melting transition from strong to weak pinning.

As seen in Fig. 6, the resulting data is highly symmetric about zero field at large fields. The hysteresis in the leading edges of the peaks are well resolved and consistent in both directions of applied field. Beyond that, we also notice a weaker hysteresis within ±0.3 T, corresponding to the Bragg glass phase, although it is barely visible in the $V''(H)$ data.

## APPENDIX C: TEMPERATURE- AND FIELD-DEPENDENCE OF $V''$ AT 20 kHz

As shown in Fig. 7, the temperature- and field-dependent screening response measurement is repeated at a drive frequency of 20 kHz at the same drive current. Since MI is proportional to both frequency and drive current, the signal amplitude is scaled down by a factor of 5. Nevertheless, we found the same nonmonotonic field dependence in screening response, consistent with the peak effect.

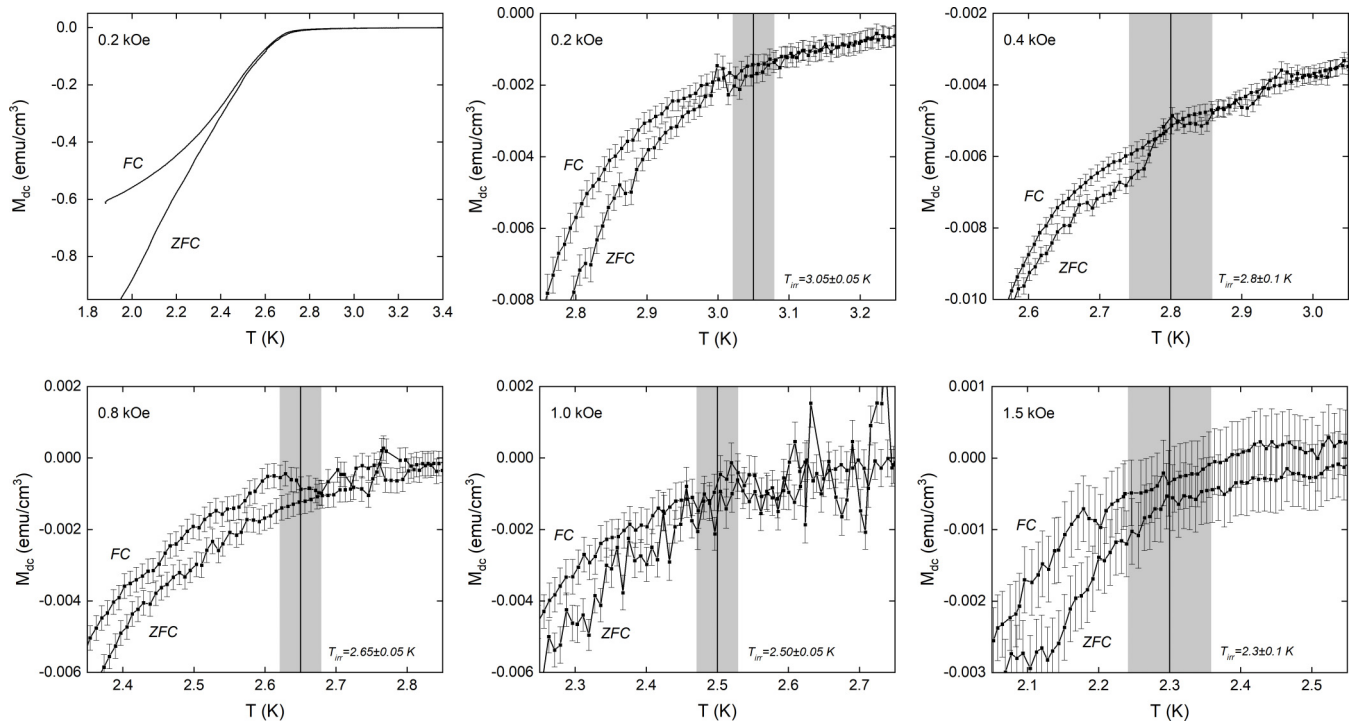


FIG. 9. Temperature dependence of dc magnetization for several $c$-axis magnetic fields. The first plot shows a comparison of FC/ZFC diamagnetic response over the full signal scale. Error bars mark the measurement uncertainty due to binning. The irreversibility temperature $T_{\rm irr}$ is defined as where the FC and ZFC curves split, with the uncertainty in locating the splitting point taken into account.

Following the same method used in the 100-kHz analysis, we extracted the features $T_{\rm knee}$, $T_{\rm break}$, $T_c$, $H_{\rm onset}$, $H_{\rm peak}$, $H_{\rm base}$, and $H_{\rm irr}$. The extracted features are plotted in Fig. 4 in the main text. While features relevant to the peak do not differ as frequency changes, the irreversibility line (i.e., the onset of the screening response) does shift to a lower temperature, as expected from a frequency-dependent activation energy for vortex depinning.

## APPENDIX D: RESISTANCE AND CURRENT-VOLTAGE CHARACTERISTICS OF $CsV_3Sb_5$

Resistance vs temperature is measured in a Quantum Design Physical Properties Measurement System (PPMS). The sample for this measurement is an approximately $2 \times 0.5 \times 0.1$ mm$^3$ $CsV_3Sb_5$ crystal (sample 2) within the same batch of samples measured by MI. Contacts were made with silver paste in a four-probe geometry. The excitation current we used for the resistance measurement is 300 μA.

As shown in Fig. 8, at zero applied magnetic field, the zero-resistance superconducting transition temperature is $T_c \approx 3.25$ K, consistent with the onset of superfluid screening response $V''$ in MI data when extrapolated to $f \to 0$ (dc). The field-dependent $T_c(H)$ is taken as the onset of the superconducting transition, where the resistance starts to deviate from its normal state value by one standard deviation of the signal fluctuation. The broadened superconducting transition suggests the crucial role of vortex dynamics in this material.

Indeed, the I-V characteristics at $T = 1.88$ K in varying magnetic fields show a strongly non-Ohmic behavior over a broad range of excitation currents, further supporting the vortex glass picture. The applied magnetic field ranges from 0 Oe (violet) to 3 kOe (red). From the I-V characteristics, we extract the critical current by vortex depinning.

## APPENDIX E: TEMPERATURE-DEPENDENCE OF DC MAGNETIZATION

The dc magnetization of another $CsV_3Sb_5$ sample (approximately $1.5 \times 1.5 \times 0.1$ mm$^3$) (sample 3) within the same batch was measured using a superconducting quantum interference device (SQUID) magnetometer in a Quantum Design Magnetic Properties Measurement System (MPMS). The sample was mounted using GE 7031 varnish such that the magnetic field is along the $c$ axis.

Magnetization was measured by the standard zero-field-cooling/field-cooling (ZFC/FC) protocol: as an example, in the first panel in Fig. 9, starting from 6 K where no superconductivity is expected, the sample was cooled in zero field (remnant field ∼0.5 Oe); at 1.8 K, we ramp up the $c$-axis magnetic field to a desired strength. ZFC data were collected during the subsequent warming to 6 K, where the full diamagnetic response relaxes to zero. Immediately following was a cooling step in the same magnetic field, during which FC data were collected as the field-trained diamagnetic response. The splitting of ZFC/FC curves was taken as the onset of irreversibility in flux pinning, and thus termed the irreversibility line $T_{\rm irr}(H)$.

The next five panels in Fig. 9 show the evolution of the irreversibility line $T_{\rm irr}(H)$. Here, the splitting of ZFC/FC occurs gradually and generally precedes the rapid increase in diamagnetic response. Therefore, we need to zoom in very closely to zero signal and, consequently, the determination of the splitting suffers from signal statistical

fluctuations. Nevertheless, with a generous error bar, we extract $T_{\rm irr}(H)$ for a handful of applied fields, which were included in the vortex phase diagram Fig. 4 in the main text.


[1] E. Fradkin, S. A. Kivelson, and J. M. Tranquada, *Colloquium:* Theory of intertwined orders in high temperature superconductors, Rev. Mod. Phys. **87**, 457 (2015).

[2] B. V. Svistunov, E. S. Babaev, and N. V. Prokof'ev, *Superfluid States of Matter* (CRC Press, Boca Raton, FL, 2015).

[3] R. M. Fernandes, P. P. Orth, and J. Schmalian, Intertwined vestigial order in quantum materials: Nematicity and beyond, Annu. Rev. Condens. Matter Phys. **10**, 133 (2019).

[4] B. R. Ortiz, S. M. L. Teicher, Y. Hu, J. L. Zuo, P. M. Sarte, E. C. Schueller, A. M. M. Abeykoon, M. J. Krogstad, S. Rosenkranz, R. Osborn, R. Seshadri, L. Balents, J. He, and S. D. Wilson, $CsV_3Sb_5$: Topological kagome metal with a superconducting ground state, Phys. Rev. Lett. **125**, 247002 (2020).

[5] B. R. Ortiz, S. M. L. Teicher, L. Kautzsch, P. M. Sarte, N. Ratcliff, J. Harter, J. P. C. Ruff, R. Seshadri, and S. D. Wilson, Fermi surface mapping and the nature of charge-density-wave order in the kagome superconductor $CsV_3Sb_5$, Phys. Rev. X **11**, 041030 (2021).

[6] D. Song, L. Zheng, F. Yu, J. Li, L. Nie, M. Shan, D. Zhao, S. Li, B. Kang, Z. Wu, Y. Zhou, K. Sun, K. Liu, X. Luo, Z. Wang, J. Ying, X. Wan, T. Wu, and X. Chen, Orbital ordering and fluctuations in a kagome superconductor $CsV_3Sb_5$, Sci. China Phys. Mech. Astron. **65**, 247462 (2022).

[7] H.-S. Xu, Y.-J. Yan, R. Yin, W. Xia, S. Fang, Z. Chen, Y. Li, W. Yang, Y. Guo, and D.-L. Feng, Multiband superconductivity with sign-preserving order parameter in kagome superconductor $CsV_3Sb_5$, Phys. Rev. Lett. **127**, 187004 (2021).

[8] R. Gupta, D. Das, C. H. Mielke III, Z. Guguchia, T. Shiroka, C. Baines, M. Bartkowiak, H. Luetkens, R. Khasanov, Q. Yin, Z. Tu, C. Gong, and H. Lei, Microscopic evidence for anisotropic multigap superconductivity in the $CsV_3Sb_5$ kagome superconductor, npj Quantum Mater. **7**, 49 (2022).

[9] H. Chen, H. Yang, B. Hu, Z. Zhao, J. Yuan, Y. Xing, G. Qian, Z. Huang, G. Li, Y. Ye, S. Ma, S. Ni, H. Zhang, Q. Yin, C. Gong, Z. Tu, H. Lei, H. Tan, S. Zhou, C. Shen *et al.*, Roton pair density wave in a strong-coupling kagome superconductor, Nature (London) **599**, 222 (2021).

[10] K. Jiang, T. Wu, J.-X. Yin, Z. Wang, M. Z. Hasan, S. D. Wilson, X. Chen, and J. Hu, Kagome superconductors $AV_3Sb_5$ ($A$ = K, Rb, Cs), Natl. Sci. Rev. **10** (2022).

[11] D. R. Saykin, C. Farhang, E. D. Kountz, D. Chen, B. R. Ortiz, C. Shekhar, C. Felser, S. D. Wilson, R. Thomale, J. Xia, and A. Kapitulnik, High resolution polar Kerr effect studies of $CsV_3Sb_5$: Tests for time-reversal symmetry breaking below the charge-order transition, Phys. Rev. Lett. **131**, 016901 (2023).

[12] L. Fu and C. L. Kane, Superconducting proximity effect and Majorana fermions at the surface of a topological insulator, Phys. Rev. Lett. **100**, 096407 (2008).

[13] D. Majer, E. Zeldov, and M. Konczykowski, Separation of the irreversibility and melting lines in $Bi_2Sr_2CaCu_2O_8$ crystals, Phys. Rev. Lett. **75**, 1166 (1995).

[14] D. Pal, D. Dasgupta, B. K. Sarma, S. Bhattacharya, S. Ramakrishnan, and A. K. Grover, Amorphization of vortex matter and indication of a reentrant peak effect in $YBa_2Cu_3O_{7-\delta}$, Phys. Rev. B **62**, 6699 (2000).

[15] S. Ni, S. Ma, Y. Zhang, J. Yuan, H. Yang, Z. Lu, N. Wang, J. Sun, Z. Zhao, D. Li, S. Liu, H. Zhang, H. Chen, K. Jin, J. Cheng, L. Yu, F. Zhou, X. Dong, J. Hu, H.-J. Gao *et al.*, Anisotropic superconducting properties of kagome metal $CsV_3Sb_5$, Chin. Phys. Lett. **38**, 057403 (2021).

[16] A. B. Pippard, A possible mechanism for the peak effect in type II superconductors, Philos. Mag. **19**, 217 (1969).

[17] A. I. Larkin and Y. N. Ovchinnikov, Pinning in type II superconductors, J. Low Temp. Phys. **34**, 409 (1979).

[18] T. Giamarchi and P. Le Doussal, Phase diagrams of flux lattices with disorder, Phys. Rev. B **55**, 6577 (1997).

[19] W. De Sorbo, The peak effect in substitutional and interstitial solid solutions of high-field superconductors, Rev. Mod. Phys. **36**, 90 (1964).

[20] T. G. Berlincourt, R. R. Hake, and D. H. Leslie, Superconductivity at high magnetic fields and current densities in some Nb-Zr alloys, Phys. Rev. Lett. **6**, 671 (1961).

[21] X. Ling and J. I. Budnick, A.C. susceptibility studies of type-ii superconductors: Vortex dynamics, in *Magnetic Susceptibility of Superconductors and Other Spin Systems*, edited by R. A. Hein, T. L. Francavilla, and D. H. Liebenberg (Springer US, Boston, MA, 1991), pp. 377–388.

[22] W. K. Kwok, J. A. Fendrich, C. J. van der Beek, and G. W. Crabtree, Peak effect as a precursor to vortex lattice melting in single crystal $YBa_2Cu_3O_{7-\delta}$, Phys. Rev. Lett. **73**, 2614 (1994).

[23] M. J. Higgins and S. Bhattacharya, Varieties of dynamics in a disordered flux-line lattice, Phys. C **257**, 232 (1996).

[24] J. Ge, J. Gutierrez, J. Li, J. Yuan, H.-B. Wang, K. Yamaura, E. Takayama-Muromachi, and V. V. Moshchalkov, Peak effect in optimally doped $p$-type single-crystal $Ba_{0.5}K_{0.5}Fe_2As_2$ studied by ac magnetization measurements, Phys. Rev. B **88**, 144505 (2013).

[25] C. V. Tomy, G. Balakrishnan, and D. M. Paul, Observation of the peak effect in the superconductor $Ca_3Rh_4Sn_{13}$, Phys. Rev. B **56**, 8346 (1997).

[26] Z. F. Weng, M. Smidman, G. M. Pang, O. Prakash, Y. Chen, Y. J. Zhang, S. Ramakrishnan, and H. Q. Yuan, Nodeless superconductivity and the peak effect in the quasiskutterudites $Lu_3Os_4Ge_{13}$ and $Y_3Ru_4Ge_{13}$, Phys. Rev. B **95**, 184501 (2017).

[27] E. H. Brandt, The flux-line lattice in superconductors, Rep. Prog. Phys. **58**, 1465 (1995).

[28] A. T. Fiory, A. F. Hebard, P. M. Mankiewich, and R. E. Howard, Penetration depths of high $T_c$ films measured by two-coil mutual inductances, Appl. Phys. Lett. **52**, 2165 (1988).

[29] B. Jeanneret, J. L. Gavilano, G. A. Racine, C. Leemann, and P. Martinoli, Inductive conductance measurements in two-dimensional superconducting systems, Appl. Phys. Lett. **55**, 2336 (1989).

[30] S. J. Turneaure, E. R. Ulm, and T. R. Lemberger, Numerical modeling of a two-coil apparatus for measuring the magnetic penetration depth in superconducting films and arrays, J. Appl. Phys. **79**, 4221 (1996).

[31] D. Chen, B. He, M. Yao, Y. Pan, H. Lin, W. Schnelle, Y. Sun, J. Gooth, L. Taillefer, and C. Felser, Anomalous thermoelectric effects and quantum oscillations in the kagome metal $CsV_3Sb_5$, Phys. Rev. B **105**, L201109 (2022).

[32] See Supplemental Material at https://link.aps.org/supplemental/10.1103/PhysRevB.109.144507 for details about the mutual inductance experiment, further mutual inductance data, and supporting transport and magnetization data.

[33] W. Duan, Z. Nie, S. Luo, F. Yu, B. R. Ortiz, L. Yin, H. Su, F. Du, A. Wang, Y. Chen, X. Lu, J. Ying, S. D. Wilson, X. Chen, Y. Song, and H. Yuan, Nodeless superconductivity in the kagome metal $CsV_3Sb_5$, Sci. China Phys. Mech. Astron. **64**, 107462 (2021).

[34] W. Zhang, X. Liu, L. Wang, C. W. Tsang, Z. Wang, S. T. Lam, W. Wang, J. Xie, X. Zhou, Y. Zhao, S. Wang, J. Tallon, K. T. Lai, and S. K. Goh, Nodeless Superconductivity in kagome metal $CsV_3Sb_5$ with and without time reversal symmetry breaking, Nano Lett. **23**, 872 (2023).

[35] K. A. Müller, M. Takashige, and J. G. Bednorz, Flux trapping and superconductive glass state in $La_2CuO_{4-y}$:Ba, Phys. Rev. Lett. **58**, 1143 (1987).

[36] N. R. Werthamer, E. Helfand, and P. C. Hohenberg, Temperature and purity dependence of the superconducting critical field, $H_{c2}$. III. Electron spin and spin-orbit effects, Phys. Rev. **147**, 295 (1966).

[37] H. Küpfer, T. Wolf, R. Meier-Hirmer, and A. Zhukov, Peak effect and vortex phase diagram in twin-free $YBa_2Cu_3O_{7-\delta}$ single crystals, Phys. C **332**, 80 (2000).

[38] T. Hanaguri, T. Tsuboi, Y. Tsuchiya, K.-I. Sasaki, and A. Maeda, Reduction of the superfluid density in the vortex-liquid phase of $Bi_2Sr_2CaCu_2O_y$, Phys. Rev. Lett. **82**, 1273 (1999).

[39] G. Blatter, M. V. Feigel'man, V. B. Geshkenbein, A. I. Larkin, and V. M. Vinokur, Vortices in high-temperature superconductors, Rev. Mod. Phys. **66**, 1125 (1994).

[40] E. Zeldov, D. Majer, M. Konczykowski, V. B. Geshkenbein, V. M. Vinokur, and H. Shtrikman, Thermodynamic observation of first-order vortex-lattice melting transition in $Bi_2Sr_2CaCu_2O_8$, Nature (London) **375**, 373 (1995).

[41] R. E. Hetzel, A. Sudbø, and D. A. Huse, First-order melting transition of an Abrikosov vortex lattice, Phys. Rev. Lett. **69**, 518 (1992).

[42] A. P. Malozemoff, T. K. Worthington, Y. Yeshurun, F. Holtzberg, and P. H. Kes, Frequency dependence of the ac susceptibility in a Y-Ba-Cu-O crystal: A reinterpretation of $H_{c2}$, Phys. Rev. B **38**, 7203 (1988).

[43] D. E. Farrell, E. Johnston-Halperin, L. Klein, P. Fournier, A. Kapitulnik, E. M. Forgan, A. I. M. Rae, T. W. Li, M. L. Trawick, R. Sasik, and J. C. Garland, Magnetization jumps and irreversibility in $Bi_2Sr_2CaCu_2O_8$, Phys. Rev. B **53**, 11807 (1996).